NASA/CR-2002-211660
ICASE Report No. 2002-20

Multiple-relaxation-time Lattice Boltzmann Models in 3D

Dominique d'Humieres
École Normale Supérieure, Paris Cédex 05, France

Irina Ginzburg
Fraunhofer-Institut für Techno- und Wirtschaftsmathematik, Kaiserslautern, Germany

Manfred Krafczyk
Technische Universität Braunschweig, Braunschweig, Germany

Pierre Lallemand
Université Paris-Sud, Orsay Cédex, France

Li-Shi Luo
ICASE, Hampton, Virginia

July 2002

The NASA STI Program Office . . . in Profile

Since its founding, NASA has been dedicated to the advancement of aeronautics and space science. The NASA Scientific and Technical Information (STI) Program Office plays a key part in helping NASA maintain this important role.

The NASA STI Program Office is operated by Langley Research Center, the lead center for NASA's scientific and technical information. The NASA STI Program Office provides access to the NASA STI Database, the largest collection of aeronautical and space science STI in the world. The Program Office is also NASA's institutional mechanism for disseminating the results of its research and development activities. These results are published by NASA in the NASA STI Report Series, which includes the following report types:

- TECHNICAL PUBLICATION. Reports of completed research or a major significant phase of research that present the results of NASA programs and include extensive data or theoretical analysis. Includes compilations of significant scientific and technical data and information deemed to be of continuing reference value. NASA's counterpart of peer-reviewed formal professional papers, but having less stringent limitations on manuscript length and extent of graphic presentations.

- TECHNICAL MEMORANDUM. Scientific and technical findings that are preliminary or of specialized interest, e.g., quick release reports, working papers, and bibliographies that contain minimal annotation. Does not contain extensive analysis.

- CONTRACTOR REPORT. Scientific and technical findings by NASA-sponsored contractors and grantees.

- CONFERENCE PUBLICATIONS. Collected papers from scientific and technical conferences, symposia, seminars, or other meetings sponsored or cosponsored by NASA.

- SPECIAL PUBLICATION. Scientific, technical, or historical information from NASA programs, projects, and missions, often concerned with subjects having substantial public interest.

- TECHNICAL TRANSLATION. English-language translations of foreign scientific and technical material pertinent to NASA's mission.

Specialized services that complement the STI Program Office's diverse offerings include creating custom thesauri, building customized data bases, organizing and publishing research results . . . even providing videos.

For more information about the NASA STI Program Office, see the following:

- Access the NASA STI Program Home Page at ***http://www.sti.nasa.gov***

- Email your question via the Internet to help@sti.nasa.gov

- Fax your question to the NASA STI Help Desk at (301) 621-0134

- Telephone the NASA STI Help Desk at (301) 621-0390

- Write to:
  NASA STI Help Desk
  NASA Center for AeroSpace Information
  7121 Standard Drive
  Hanover, MD 21076-1320

NASA/CR-2002-211660
ICASE Report No. 2002-20

Multiple-relaxation-time Lattice Boltzmann Models in 3D

Dominique d'Humieres
École Normale Supérieure, Paris Cédex 05, France

Irina Ginzburg
Fraunhofer-Institut für Techno- und Wirtschaftsmathematik, Kaiserslautern, Germany

Manfred Krafczyk
Technische Universität Braunschweig, Braunschweig, Germany

Pierre Lallemand
Université Paris-Sud, Orsay Cédex, France

Li-Shi Luo
ICASE, Hampton, Virginia

ICASE
NASA Langley Research Center
Hampton, Virginia
Operated by Univerities Space Research Association

Prepared for Langley Research Center
under Contract NAS1-97046

July 2002

Available from the following:

NASA Center for AeroSpace Information (CASI)
7121 Standard Drive
Hanover, MD 21076-1320
(301) 621-0390

National Technical Information Service (NTIS)
5285 Port Royal Road
Springfield, VA 22161-2171
(703) 487-4650

MULTIPLE-RELAXATION-TIME LATTICE BOLTZMANN MODELS IN 3D

DOMINIQUE D'HUMIÈRES*, IRINA GINZBURG†, MANFRED KRAFCZYK‡, PIERRE LALLEMAND§, AND LI-SHI LUO¶

Abstract. This article provides a concise exposition of the multiple-relaxation-time lattice Boltzmann equation, with examples of fifteen-velocity and nineteen-velocity models in three dimensions. Simulation of a diagonally lid-driven cavity flow in three dimensions at Re = 500 and 2000 is performed. The results clearly demonstrate the superior numerical stability of the multiple-relaxation-time lattice Boltzmann equation over the popular lattice Bhatnagar-Gross-Krook equation.

Key words. multiple-relaxation-time LBE in 3D, D3Q15 and D3Q19 models, 3D diagonal lid driven cavity flow

Subject classification. Fluid Mechanics

1. Introduction. The relaxation lattice Boltzmann equation (RLBE) was introduced by Higuera and Jiménez [20] to overcome some drawbacks of lattice gas automata (LGA) such as large statistical noise, limited range of physical parameters, non-Galilean invariance, and implementation difficulty in three dimensions. In the original RLBE the equilibria and the relaxation matrix were derived from the underlying LGA models. It was soon realized that the connection to the LGA model could be abandoned and the equilibria and collision matrices could be constructed independently to better suit numerics [21].

The simplest lattice Boltzmann equation (LBE) is the lattice Bhatnagar-Gross-Krook (BGK) equation, based on a single-relaxation-time approximation [1]. Due to its extreme simplicity, the lattice BGK (LBGK) equation [29, 4] has become the most popular lattice Boltzmann model in spite of its well known deficiencies.

The multiple-relaxation-time (MRT) lattice Boltzmann equation was also developed at the same time [7]. The MRT lattice Boltzmann equation (also referred to as the generalized lattice Boltzmann equation (GLBE) or the moment method) overcomes some obvious defects of the LBGK model, such as fixed Prandtl number (Pr = 1 for the BGK model) and fixed ratio between the kinematic and bulk viscosities. The MRT lattice Boltzmann equation has been persistently pursued, and much progress has been made. Successes include: formulation of optimal boundary conditions [10, 22], interface conditions in multi-phase flows [11] and free surfaces [12], thermal [26] and viscoelastic models [13, 14], models with reduced lattice symmetries [8, 2], and improvement of numerical stability [23]. It should be stressed that most of the above results cannot be obtained with the LBGK models. Applying optimization techniques in coding, the computational efficiency of the RLBE method [7] can be fairly close to that of the LBGK method for most practical applications

*Laboratoire de Physique Statistique, École Normale Supérieure, 24 Rue Lhomond, 75231 Paris Cédex 05, France.

†Fraunhofer-Institut für Techno- und Wirtschaftsmathematik, Gottlieb-Daimler-Straße 49, D-67663 Kaiserslautern, Germany.

‡Institut für Computeranwendungen im Bauingenieurwesen, Technische Universität Braunschweig, Pockelsstraße 3, D-38106 Braunschweig, Germany.

§Laboratoire Applications Scientifiques du Calcul Intensif (ASCI), Bâtiment 506, Université Paris-Sud (Paris XI Orsay), 91405 Orsay Cédex, France.

¶ICASE, Mail Stop 132C, NASA Langley Research Center, 3 West Reid Street, Building 1152, Hampton, VA 23681-2199 (email address: luo@icase.edu). This research was supported by the National Aeronautics and Space Administration under NASA Contract No. NAS1-97046 while the author was in residence at ICASE, NASA Langley Research Center, Hampton, VA 23681-2199.

(RLBE schemes could be *ca.* 15% slower than their LBGK counterparts in terms of the number of sites updated per second). Recently it was shown that the multiple-relaxation-time LBE models are much more stable than their LBGK counterparts (Lallemand & Luo 2000), because the different relaxation times can be individually tuned to achieve 'optimal' stability.

In this paper we intend to bring attention to the multiple-relaxation-time LBE by demonstrating its superior stability to LBGK models. This paper is organized as follows. Section 2 briefly outlines the basic theory of the multiple-relaxation-time LBE. Section 3 provides as a 'template' example: a fifteen-velocity RLBE model in three dimensions (D3Q15 model). Section 4 gives some results for a three-dimensional cavity flow simulated by using both RLBE and LBGK methods. Finally, section 5 concludes the paper. The appendix briefly describes the nineteen-velocity model in three dimensions (D3Q19 model).

2. Multiple-relaxation-time lattice Boltzmann equation. Although it can be shown that the lattice Boltzmann equation is a finite difference form of the linearized continuous Boltzmann equation [17, 18], we present RLBE as a self-contained mathematical object representing a dynamical system with a finite number of moments in discrete space and time.

The general RLBE model has three components. The first component is discrete phase space defined by a regular lattice in D dimensions together with a set of *judiciously chosen* discrete velocities $\{\boldsymbol{e}_\alpha | \alpha = 0, 1, \ldots, N\}$ connecting each lattice site to some of its neighbours. The fundamental object in the theory is the set of velocity distribution functions $\{f_\alpha | \alpha = 0, 1, \ldots, N\}$ defined on each node $\boldsymbol{r}_i$ of the lattice. The second component includes a collision matrix S and $(N+1)$ equilibrium distribution functions $\{f_\alpha^{(\mathrm{eq})} | \alpha = 0, 1, \ldots, N\}$. The equilibrium distribution functions are functions of the local conserved quantities. The third component is the evolution equation in discrete time $t_n = n\delta t$, $n = 0, 1, \ldots$,

$$|f(\boldsymbol{r}_i + \boldsymbol{e}_\alpha \delta t,\, t + \delta t)\rangle - |f(\boldsymbol{r}_i,\, t)\rangle = -\mathsf{S}\left[\, |f(\boldsymbol{r}_i,\, t)\rangle - |f^{(\mathrm{eq})}(\boldsymbol{r}_i,\, t)\rangle \,\right]. \tag{2.1}$$

In the above equation we have used the following notations for column vectors in $(N+1)$-dimensional space $\mathbb{V} = \mathbb{R}^{N+1}$,

$$\begin{aligned}
&|f(\boldsymbol{r}_i,\, t)\rangle \equiv (f_0(\boldsymbol{r}_i,\, t),\, f_1(\boldsymbol{r}_i,\, t),\, \ldots,\, f_N(\boldsymbol{r}_i,\, t))^{\mathsf{T}}, \\
&|f^{(\mathrm{eq})}(\boldsymbol{r}_i,\, t)\rangle \equiv (f_0^{(\mathrm{eq})}(\boldsymbol{r}_i,\, t),\, f_1^{(\mathrm{eq})}(\boldsymbol{r}_i,\, t),\, \ldots,\, f_N^{(\mathrm{eq})}(\boldsymbol{r}_i,\, t))^{\mathsf{T}}, \quad \text{and} \\
&|f(\boldsymbol{r}_i + \boldsymbol{e}_\alpha \delta t,\, t + \delta t)\rangle \equiv (f_0(\boldsymbol{r}_i,\, t + \delta t),\, \ldots,\, f_N(\boldsymbol{r}_i + \boldsymbol{e}_N \delta t,\, t + \delta t))^{\mathsf{T}},
\end{aligned}$$

where T denotes the transpose operator and we always assume that $\boldsymbol{e}_0 \equiv \boldsymbol{0}$. From here on the Dirac notations of bra $\langle\cdot|$ and ket $|\cdot\rangle$ vectors are used to denote respectively the row and column vectors. Note that equation (2.1) is written in such a way that its right- and left-hand-sides represent the two elementary steps in the evolution of the lattice Boltzmann equation: advection and collision. The advection process is naturally executed in velocity space $\mathbb{V}$, $f_\alpha(\boldsymbol{r}_i,\, t)$ being simply shifted in space according to the velocity $\boldsymbol{e}_\alpha$ to $f_\alpha(\boldsymbol{r}_i + \boldsymbol{e}_\alpha \delta t,\, t + \delta t)$. The collision process is naturally accomplished in the space spanned by the eigenvectors of the collision matrix, the corresponding eigenvalues being the inverse of their relaxation time towards their equilibria. The $(N+1)$ eigenvalues of S are all between 0 and 2 so as to maintain linear stability and the separation of scales, which means that the relaxation times of non-conserved quantities are much faster than the hydrodynamic time scales. The LBGK models are special cases in which the $(N+1)$ relaxation times are all equal, and the collision matrix $\mathsf{S} = \omega \mathsf{I}$, where I is the identity matrix, $\omega = 1/\tau$, and τ $(> 1/2)$ is the single relaxation time of the model.

To simulate athermal fluids, a necessary criterion is that the discrete velocity set must be sufficient to represent a scalar (mass density ρ), a vector (momentum $\boldsymbol{j}$), another scalar (pressure P), and a symmetric

traceless second rank tensor (viscous stress tensor σ_{ij}). More generally, the velocity set must possess sufficient symmetries for the hydrodynamic equations to hold: the conserved quantities and their fluxes must transform properly so that they can approximate their continuous counterparts in an appropriate limit. Finally the local conserved quantities must be the mass density ρ and the momentum $\boldsymbol{j}$ for athermal fluids.

Given a chosen set of discrete velocities $\{\boldsymbol{e}_\alpha | \alpha = 0, 1, \ldots, N\}$ and corresponding distribution functions $\{f_\alpha | \alpha = 0, 1, \ldots, N\}$, an equal number of moments $\{m_\beta | \beta = 0, 1, \ldots, N\}$ of the distribution functions f_α can be obtained as

$$m_\beta \equiv \langle \phi_\beta | f \rangle = \langle f | \phi_\beta \rangle, \quad \langle f | = (f_0, f_1, \ldots, f_N), \tag{2.2}$$

where $\{|\phi_\beta\rangle | \beta = 0, 1, \ldots, N\}$ is an orthogonal dual basis set constructed by the Gram-Schmidt orthogonalization procedure (*e.g.* Bouzidi *et al.* 2001*a*) from polynomials of the column vectors $|e_{x_i}\rangle$ in space $\mathbb{V}$. Vector $|e_{x_i}\rangle$ is built from the components of the $\boldsymbol{e}_\alpha$'s, *i.e.* $|e_{x_i}\rangle \equiv (e_{0\,x_i}, e_{1\,x_i}, \ldots, e_{N\,x_i})^{\mathsf{T}}$, for $i \in \{1, 2, \ldots, D\}$ in D dimensions (*e.g.*, $\{|e_x\rangle, |e_y\rangle, |e_z\rangle\}$ in three dimensions).

The set $\{|\phi_\beta\rangle\}$ is analogous to the Hermite tensor polynomials in continuous velocity space [15, 16]. It should be stressed that the orthogonal functions defined on a finite set of discrete velocities $\{\boldsymbol{e}_\alpha\}$ has some degeneracies which do not exist in the Hermite tensor polynomials in continuous space. Obviously, the moments are simply linear combinations of the f_α's, therefore velocity space $\mathbb{V}$, spanned by $|f\rangle \equiv (f_0, f_1, \ldots, f_N)^{\mathsf{T}}$, and the moment space $\mathbb{M}$, spanned by $|m\rangle \equiv (m_0, m_1, \ldots, m_N)^{\mathsf{T}}$, are related by a linear mapping M: $|m\rangle = \mathsf{M}|f\rangle$ and $|f\rangle = \mathsf{M}^{-1}|m\rangle$. The transformation matrix M would be an orthogonal transformation if the basis vectors $\{|\phi_\beta\rangle\}$ are normalized.

If the matrix S is chosen such that the $\{|\phi_\beta\rangle\}$ are its eigenvectors, the linear relaxation of the kinetic modes in moment space $\mathbb{M}$ naturally accomplishes the collision process. Then the evolution equation (2.1) of the multiple-relaxation-time lattice Boltzmann equation becomes [7, 23]:

$$|f(\boldsymbol{r}_i + \boldsymbol{e}_\alpha \delta t,\, t + \delta t)\rangle - |f(\boldsymbol{r}_i,\, t)\rangle = -\mathsf{M}^{-1}\widehat{\mathsf{S}} \left[\, |m(\boldsymbol{r}_i,\, t)\rangle - |m^{(\mathrm{eq})}(\boldsymbol{r}_i,\, t)\rangle \, \right], \tag{2.3}$$

where the collision matrix $\widehat{\mathsf{S}} = \mathsf{M} \cdot \mathsf{S} \cdot \mathsf{M}^{-1}$ is diagonal: $\widehat{\mathsf{S}} \equiv \mathrm{diag}(s_0, s_1, \ldots, s_N)$, and $m_\alpha^{(\mathrm{eq})}$ is the equilibrium value of the moment m_α. The $(N+1)$ moments can be separated into two groups: the 'hydrodynamic' (conserved) moments and the 'kinetic' (non-conserved) moments. The first group consists of the moments locally conserved in the collision process, so that in general $m_\beta^{(\mathrm{eq})} = m_\beta$. The second group consists of the moments not conserved in the collision process so that $m_\beta^{(\mathrm{eq})} \neq m_\beta$. The equilibria $\{m_\beta^{(\mathrm{eq})}\}$ are functions of the conserved moments and are invariant under the symmetry group of the underlying lattice. For models designed to simulate athermal fluids, the only hydrodynamic moments are mass density ρ (a scalar) and momentum $\boldsymbol{j}$ (a vector): energy is not a conserved quantity for athermal fluids. Equilibrium values of kinetic moments are functions of ρ and $\|\boldsymbol{j}\|^2$ for scalars, and $\boldsymbol{j}$ times some functions of ρ and $\|\boldsymbol{j}\|^2$ (eventually a constant) for vectors, and so on, as discussed in §3.

From the above definition of the conserved and non-conserved moments, Eq. (2.3) can be rewritten as

$$|f(\boldsymbol{r}_i + \boldsymbol{e}_\alpha \delta t,\, t + \delta t)\rangle - |f(\boldsymbol{r}_i,\, t)\rangle = -\sum_{\beta \in B^{(\mathrm{K})}} \frac{s_\beta}{\langle \phi_\beta | \phi_\beta \rangle} [(m_\beta(\boldsymbol{r}_i,\, t) - m_\beta^{(\mathrm{eq})}(\boldsymbol{r}_i,\, t))] \, |\phi_\beta\rangle, \tag{2.4}$$

where we have used the fact that $(\mathsf{M} \cdot \mathsf{M}^{\mathsf{T}})$ is a diagonal matrix with diagonal elements $\langle \phi_\beta | \phi_\beta \rangle$. It is obvious that the actual values of the s_β's for conserved moments are irrelevant, because $m_\beta^{(\mathrm{eq})}(\boldsymbol{r}_i,\, t) = m_\beta(\boldsymbol{r}_i,\, t)$ for $\beta \in B^{(\mathrm{H})}$ by definition, but they are set to zero in general in what follows. Note that this point is purely academic in the present context, but is very important when including body forces, as shown by Ginzbourg and Adler [10].

The RLBE formulation has two important consequences. First, one has the maximum number of adjustable relaxation times, one for each class of kinetic modes invariant under the symmetry group of the underlying lattice. Second, one has maximum freedom in the construction of the equilibrium functions of the non-conserved moments. One immediate result of using the RLBE instead of the LBGK model is a significant improvement in numerical stability [23]. It should be emphasized that the above procedures are general and are independent of the number of discrete velocities and the number of space dimensions.

3. Multiple-relaxation-time D3Q15 model. Each point on a unit cubic lattice space has six nearest neighbours, (±1, 0, 0), (0, ±1, 0), and (0, 0, ±1), twelve next nearest neighbours, (±1, ±1, 0), (±1, 0, ±1), and (0, ±1, ±1), and eight third nearest neighbours, (±1, ±1, ±1). Elementary discrete velocity sets for lattice Boltzmann models in three dimensions are constructed from the set of twenty-six vectors pointing from the origin to the above neighbours and the zero vector $(0, 0, 0)$. The twenty-seven velocities are usually grouped into four subsets labelled by their squared modulus, 0, 1, 2, and 3. We also use the notation DdQq for the q-velocity model in d-dimensional space in what follows [29]. The D3Q15 model uses the velocity subsets 0, 1, and 3 and is described here as an example. The D3Q19 model uses the subsets 0, 1, and 2 and is described in the appendix. The D3Q13 model introduced by d'Humières *et al.* [8] only uses the subsets 0 and 2.

The fifteen discrete velocities in the D3Q15 model are

$$\boldsymbol{e}_\alpha = \begin{cases} (0,\,0,\,0), & \alpha = 0, \\ (\pm1,\,0,\,0),\ (0,\,\pm1,\,0),\ (0,\,0,\,\pm1), & \alpha = 1,\ 2,\ \ldots,\ 6, \\ (\pm1,\,\pm1,\,\pm1), & \alpha = 7,\ 8,\ \ldots,\ 14. \end{cases} \tag{3.1}$$

The components of the corresponding fifteen orthogonal basis vectors $|\phi_\beta\rangle_\alpha$ are given by:

$$\left.\begin{aligned} |\phi_0\rangle_\alpha &= \|\boldsymbol{e}_\alpha\|^0, \\ |\phi_1\rangle_\alpha &= \|\boldsymbol{e}_\alpha\|^2 - 2, \\ |\phi_2\rangle_\alpha &= \tfrac{1}{2}(15\|\boldsymbol{e}_\alpha\|^4 - 55\|\boldsymbol{e}_\alpha\|^2 + 32), \end{aligned}\right\} \tag{3.2a}$$

$$\left.\begin{aligned} |\phi_3\rangle_\alpha &= e_{\alpha x}, \\ |\phi_5\rangle_\alpha &= e_{\alpha y}, \\ |\phi_7\rangle_\alpha &= e_{\alpha z}, \end{aligned}\right\} \tag{3.2b}$$

$$\left.\begin{aligned} |\phi_4\rangle_\alpha &= \tfrac{1}{2}(5\|\boldsymbol{e}_\alpha\|^2 - 13)e_{\alpha x}, \\ |\phi_6\rangle_\alpha &= \tfrac{1}{2}(5\|\boldsymbol{e}_\alpha\|^2 - 13)e_{\alpha y}, \\ |\phi_8\rangle_\alpha &= \tfrac{1}{2}(5\|\boldsymbol{e}_\alpha\|^2 - 13)e_{\alpha z}, \end{aligned}\right\} \tag{3.2c}$$

$$\left.\begin{aligned} |\phi_9\rangle_\alpha &= 3e_{\alpha x}^2 - \|\boldsymbol{e}_\alpha\|^2, \\ |\phi_{10}\rangle_\alpha &= e_{\alpha y}^2 - e_{\alpha z}^2, \end{aligned}\right\} \tag{3.2d}$$

$$\left.\begin{aligned} |\phi_{11}\rangle_\alpha &= e_{\alpha x}e_{\alpha y}, \\ |\phi_{12}\rangle_\alpha &= e_{\alpha y}e_{\alpha z}, \\ |\phi_{13}\rangle_\alpha &= e_{\alpha x}e_{\alpha z}, \end{aligned}\right\} \tag{3.2e}$$

$$|\phi_{14}\rangle_\alpha = e_{\alpha x}e_{\alpha y}e_{\alpha z}, \tag{3.2f}$$

where $\alpha \in \{0, 1, \ldots, 14\}$, $\|\boldsymbol{e}_\alpha\| = (e_{\alpha x}^2 + e_{\alpha y}^2 + e_{\alpha z}^2)^{1/2}$ and $\|\boldsymbol{e}_0\|^0 = 1$. The orthogonal basis set $\{|\phi_\beta\rangle\}$ is obtained by orthogonalizing the polynomials of the column vectors $|e_{x_i}\rangle$ by the standard Gram-Schmidt procedure (*e.g.* [2])). The corresponding fifteen moments $\{m_\beta|\beta = 0,\ 1,\ \ldots,\ 14\}$ are: the mass density ($m_0 = \rho$), the part of the kinetic energy independent of the density ($m_1 = e$), the part of the kinetic energy

square independent of the density and kinetic energy ($m_2 = \epsilon = e^2$), the momentum ($m_{3,5,7} = j_{x,y,z}$), the energy flux independent of the mass flux ($m_{4,6,8} = q_{x,y,z}$), the symmetric traceless viscous stress tensor ($m_9 = 3p_{xx}$, $m_{10} = p_{ww} = p_{yy} - p_{zz}$, with $p_{xx} + p_{yy} + p_{zz} = 0$, $m_{11,12,13} = p_{xy,yz,zx}$), and an antisymmetric third-order moment ($m_{14} = m_{xyz}$), corresponding to the following order:

$$|m\rangle = (\rho,\, e,\, \epsilon,\, j_x,\, q_x,\, j_y,\, q_y,\, j_z, q_z,\, 3p_{xx},\, p_{ww},\, p_{xy},\, p_{yz},\, p_{zx},\, m_{xyz})^{\mathsf{T}}.$$

The collision matrix $\widehat{\mathsf{S}}$ in moment space $\mathbb{M}$ is the diagonal matrix

$$\widehat{\mathsf{S}} \equiv \mathrm{diag}(0,\, s_1,\, s_2,\, 0,\, s_4,\, 0,\, s_4,\, 0,\, s_4,\, s_9,\, s_9,\, s_{11},\, s_{11},\, s_{11},\, s_{14}), \tag{3.3}$$

zeros corresponding to conserved moments in the order chosen. And the matrix M is then given by

$$\mathsf{M} = \begin{vmatrix}
1 & 1 & 1 & 1 & 1 & 1 & 1 & 1 & 1 & 1 & 1 & 1 & 1 & 1 & 1 \\
-2 & -1 & -1 & -1 & -1 & -1 & -1 & 1 & 1 & 1 & 1 & 1 & 1 & 1 & 1 \\
16 & -4 & -4 & -4 & -4 & -4 & -4 & 1 & 1 & 1 & 1 & 1 & 1 & 1 & 1 \\
0 & 1 & -1 & 0 & 0 & 0 & 0 & 1 & -1 & 1 & -1 & 1 & -1 & 1 & -1 \\
0 & -4 & 4 & 0 & 0 & 0 & 0 & 1 & -1 & 1 & -1 & 1 & -1 & 1 & -1 \\
0 & 0 & 0 & 1 & -1 & 0 & 0 & 1 & 1 & -1 & -1 & 1 & 1 & -1 & -1 \\
0 & 0 & 0 & -4 & 4 & 0 & 0 & 1 & 1 & -1 & -1 & 1 & 1 & -1 & -1 \\
0 & 0 & 0 & 0 & 0 & 1 & -1 & 1 & 1 & 1 & 1 & -1 & -1 & -1 & -1 \\
0 & 0 & 0 & 0 & 0 & -4 & 4 & 1 & 1 & 1 & 1 & -1 & -1 & -1 & -1 \\
0 & 2 & 2 & -1 & -1 & -1 & -1 & 0 & 0 & 0 & 0 & 0 & 0 & 0 & 0 \\
0 & 0 & 0 & 1 & 1 & -1 & -1 & 0 & 0 & 0 & 0 & 0 & 0 & 0 & 0 \\
0 & 0 & 0 & 0 & 0 & 0 & 0 & 1 & -1 & -1 & 1 & 1 & -1 & -1 & 1 \\
0 & 0 & 0 & 0 & 0 & 0 & 0 & 1 & 1 & -1 & -1 & -1 & -1 & 1 & 1 \\
0 & 0 & 0 & 0 & 0 & 0 & 0 & 1 & -1 & 1 & -1 & -1 & 1 & -1 & 1 \\
0 & 0 & 0 & 0 & 0 & 0 & 0 & 1 & -1 & -1 & 1 & -1 & 1 & 1 & -1
\end{vmatrix}. \tag{3.4}$$

Note that the row vectors of M, $\{\langle\phi_\beta|\}$, are orthogonal to each other but they are not normalized, *i.e.* $\langle\phi_\alpha|\phi_\beta\rangle = \|\phi_\alpha\| \cdot \|\phi_\beta\| \cdot \delta_{\alpha\beta}$. Note also that, with different ordering and normalization, the basis vectors $\{|\phi_k\rangle\}$ given by Ginzburg [9] are the same as the ones given here, except $|\phi_1\rangle$ and $|\phi_2\rangle$ which are replaced by an orthogonal linear combination. This would make a difference only when $s_1 \neq s_2$. The 4th, 6th, and 8th row vectors of M (corresponding to j_x, j_y, and j_z, respectively) uniquely define the ordering (or labelling) of the velocity set $\{\boldsymbol{e}_\alpha\}$ in subscript α.

With $c_s^2 = 1/3$ (c_s is the sound speed) and $s_9 = s_{11}$, the equilibria of the kinetic moments as functions of $\rho^{(\mathrm{eq})} = \rho$ and $\boldsymbol{j}^{(\mathrm{eq})} = \boldsymbol{j}$ up to second-order are given by

$$e^{(\mathrm{eq})} = -\rho + \frac{1}{\rho_0}\boldsymbol{j}\cdot\boldsymbol{j} = -\rho + \frac{1}{\rho_0}(j_x^2 + j_y^2 + j_z^2), \tag{3.5a}$$

$$\epsilon^{(\mathrm{eq})} = -\rho, \tag{3.5b}$$

$$q_x^{(\mathrm{eq})} = -\frac{7}{3}j_x, \qquad q_y^{(\mathrm{eq})} = -\frac{7}{3}j_y, \qquad q_z^{(\mathrm{eq})} = -\frac{7}{3}j_z, \tag{3.5c}$$

$$p_{xx}^{(\mathrm{eq})} = \frac{1}{3\rho_0}\left[2j_x^2 - (j_y^2 + j_z^2)\right], \qquad p_{ww}^{(\mathrm{eq})} = \frac{1}{\rho_0}\left[j_y^2 - j_z^2\right], \tag{3.5d}$$

$$p_{xy}^{(\mathrm{eq})} = \frac{1}{\rho_0}j_x j_y, \qquad p_{yz}^{(\mathrm{eq})} = \frac{1}{\rho_0}j_y j_z, \qquad p_{xz}^{(\mathrm{eq})} = \frac{1}{\rho_0}j_x j_z, \tag{3.5e}$$

$$m_{xyz}^{(\mathrm{eq})} = 0. \tag{3.5f}$$

The constants are defined as follows. The constant ρ_0 is the mean density in the system and is usually set to be unity in simulations. The approximation of $1/\rho \approx 1/\rho_0$ is used in equations (3.5a), (3.5d), and (3.5e) to reduce compressibility effects in the model (He & Luo 1997*c*). If the usual compressible Navier-Stokes equations are required, one only has to replace ρ_0 by ρ. Equation (3.5b) has the general form $\epsilon^{(\mathrm{eq})} = w_\epsilon\, \rho + w_{\epsilon j}\, \boldsymbol{j} \cdot \boldsymbol{j}/\rho_0$, where w_ϵ and $w_{\epsilon j}$ are free parameters which do not have much effect on the asymptotic Navier-Stokes equation simulated by the model. In this model, we set $w_\epsilon = -1$ and $w_{\epsilon j} = 0$; to recover the LBGK model, one must set $w_\epsilon = 1$ and $w_{\epsilon j} = -5$.

The above equilibrium functions are obtained by optimizing the isotropy and Galilean invariance of the model. The details are described in [23]. The kinematic viscosity ν and the bulk viscosity ζ of the model are

$$\nu = \frac{1}{3}\left(\frac{1}{s_9} - \frac{1}{2}\right) = \frac{1}{3}\left(\frac{1}{s_{11}} - \frac{1}{2}\right), \tag{3.6a}$$

$$\zeta = \frac{(5 - 9c_s^2)}{9}\left(\frac{1}{s_1} - \frac{1}{2}\right) = \frac{2}{9}\left(\frac{1}{s_1} - \frac{1}{2}\right). \tag{3.6b}$$

We emphasize that the above formulae are obtained under the conditions that $s_9 = s_{11}$ and $\boldsymbol{q}^{(\mathrm{eq})}$ of equation (3.5c), which are the results of the optimization, and the mean fluid velocity $\boldsymbol{V} = \boldsymbol{0}$. Corrections to these transport coefficients for finite $\boldsymbol{k}$ and non-zero mean velocity $\boldsymbol{V}$ can be calculated from the solution of the linearized dispersion equation of the system, which is equivalent to the standard von Neumann stability analysis [23].

Some properties of the lattice Boltzmann equation are dictated by the symmetries of the discrete velocity set and the simplicity of the dynamics on the lattice. One consequence is the existence of spurious invariants that may lead to some undesirable artifacts in simulations, especially near boundaries. One such invariant is the staggered invariant in LGA and LBE models [30]. The D3Q15 model has also another special invariant not found in most LBE models: the parity $\chi(\boldsymbol{r}_i)$ of a vector $\boldsymbol{r}_i = (x_i,\, y_i,\, z_i)$ defined on a three-dimensional cubic lattice by

$$\chi(\boldsymbol{r}_i) = (x_i + y_i + z_i) \pmod 2, \quad \text{for } \boldsymbol{r}_i \in \mathbb{Z}^3. \tag{3.7}$$

For the D3Q15 model, if $\chi(\boldsymbol{r}_i)$ is 0 ($\boldsymbol{r}_i \in \mathbb{Z}^3_{\mathrm{e}}$), then $\chi(\boldsymbol{r}_i + \boldsymbol{e}_\alpha)$ is 1 ($\boldsymbol{r}_i \in \mathbb{Z}^3_{\mathrm{o}}$) for $\boldsymbol{e}_\alpha \neq \boldsymbol{0}$, and *vice versa*. This means that the system has two decoupled sub-lattices ($\mathbb{Z}^3_{\mathrm{o}}$ and $\mathbb{Z}^3_{\mathrm{e}}$) for momentum, and these two sub-lattices can be coupled through boundary conditions. Consequently the system has a chequerboard (parity) invariance and one should be aware of this fact when using the D3Q15 models, especially when short-wavelength oscillations are observed in simulations. The oscillations due to the checkerboard invariance often causes numerical instability in simulations. In contrast, the D3Q19 model with velocities of parities 0 and 1 does not have this checkerboard invariance.

4. Simulations. In order to demonstrate the enhanced stability of the RLBE approach, we simulated a diagonally lid-driven cavity flow [28] with a flow configuration shown in figure 1. The mesh is uniform and of size 52^3. The boundary condition (BC) at the top plane (at $y = 1$) is $\boldsymbol{U}_{BC} = -(\sqrt{2},\, 0,\, \sqrt{2})/20$, so that $U_{BC} = \|\boldsymbol{U}_{BC}\| = 0.1$ in lattice units. The other five planes were subject to no-slip boundary conditions.

The relaxation parameters used in the RLBE simulations are $\rho_0 = 1$, $s_1 = 1.6$, $s_2 = 1.2$, $s_4 = 1.6$, and $s_{14} = 1.2$. The values of the relaxation parameters (s_α) and the adjustable parameters in $\epsilon^{(\mathrm{eq})}$ (w_ϵ and $w_{\epsilon j}$) have been obtained to attain optimal numerical stability but can only be regarded as 'sub-optimal' values which are the result of a compromise between the expected range for the Reynolds number and the effort required to find the optimal values by searching a large parameter space through *linear* analysis. These

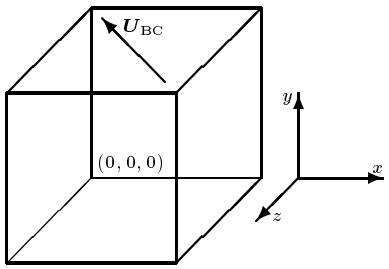

FIG. 1. *Diagonally driven cavity flow*

parameters are not adjusted to the actual Reynolds number in each simulation, but are kept constant once chosen. The relaxation parameters $s_9 = s_{11}$ are determined by the viscosity from equation (3.6a). The accuracy of the simulation is also enhanced by using, instead of the variable ρ, its fluctuations $\delta\rho \equiv \rho - \rho_0$.

The boundary conditions on the top plane are obtained in velocity space by assigning $\{f_\alpha\}$ to [22]

$$f_\alpha = w_\alpha \rho_0 \frac{\boldsymbol{e}_\alpha \cdot \boldsymbol{U}_{BC}}{c_s^2}, \tag{4.1}$$

where $w_\alpha = 1/9$ for $\alpha \in \{1, \ldots, 6\}$ and $w_\alpha = 1/72$ for $\alpha \in \{7, \ldots, 14\}$. It should be stressed that this particular implementation of a sliding boundary imposes a constant pressure $p_0 = c_s^2 \rho_0$ at the boundary, which is incorrect; and the momentum transfer in the direction perpendicular to the moving lid is significantly weakened. The correct boundary conditions consistent with the bounce-back boundary conditions should be [24, 25, 3]:

$$f_{\bar{\alpha}} = f_\alpha + 2 w_\alpha \rho_0 \frac{\boldsymbol{e}_{\bar{\alpha}} \cdot \boldsymbol{U}_{BC}}{c_s^2} = f_\alpha - 2 w_\alpha \rho_0 \frac{\boldsymbol{e}_\alpha \cdot \boldsymbol{U}_{BC}}{c_s^2}, \tag{4.2}$$

where $f_{\bar{\alpha}}$ is the distribution function of $\bar{\boldsymbol{e}}_\alpha \equiv -\boldsymbol{e}_\alpha$. Nevertheless, the implementation prescribed by equation (4.1) does help to enhance the stability of the D3Q15 model. The 'node' bounce-back boundary conditions are applied to the rest five walls for no-slip boundary conditions [6]. The 'node' bounce-back boundary conditions differ from the 'link' bounce-back boundary conditions by a one-step delay in time but otherwise they are the same. This one-time-step delay seems to effectively reduce oscillations caused by the parity invariance and thus enhances the numerical stability [5].

As the effective width of the system is approximately 50 lattice units, the Reynolds number $\mathrm{Re} = 50 U_{BC}/\nu$ was set by varying the viscosity ν. We computed the lower bounds of the viscosity for this particular flow by using the RLBE and LBGK schemes. The lower bounds are $0.6 \cdot 10^{-3}$ for RLBE scheme and $2.5 \cdot 10^{-3}$ for LBGK scheme with the identical discretization, initial and boundary conditions. Viscosities smaller than these bounds would lead to numerical instability in the simulation. Hence for our test problem with the same mesh size, the maximum Reynolds number attainable by using the RLBE scheme is about four-times that attainable using the LBGK scheme.

For the Povitsky cavity flow [28] at a low Reynolds number $\mathrm{Re} = 500$ (viscosity $\nu = 0.01$), the pressure field computed by the LBGK scheme shows severe oscillations throughout the entire computational domain, even in locations far away from the corner singularities, in contrast to the much smoother pressure field obtained by using the RLBE scheme, as depicted in figure 2.

When the Reynolds number is increased to 2000, the solution obtained by using the RLBE scheme agrees reasonably well with that obtained by using the commercial software FLUENT with a *non-uniform* 68^3 mesh [28], as shown in figure 3, even though the RLBE grid resolution is much coarser. At a relatively

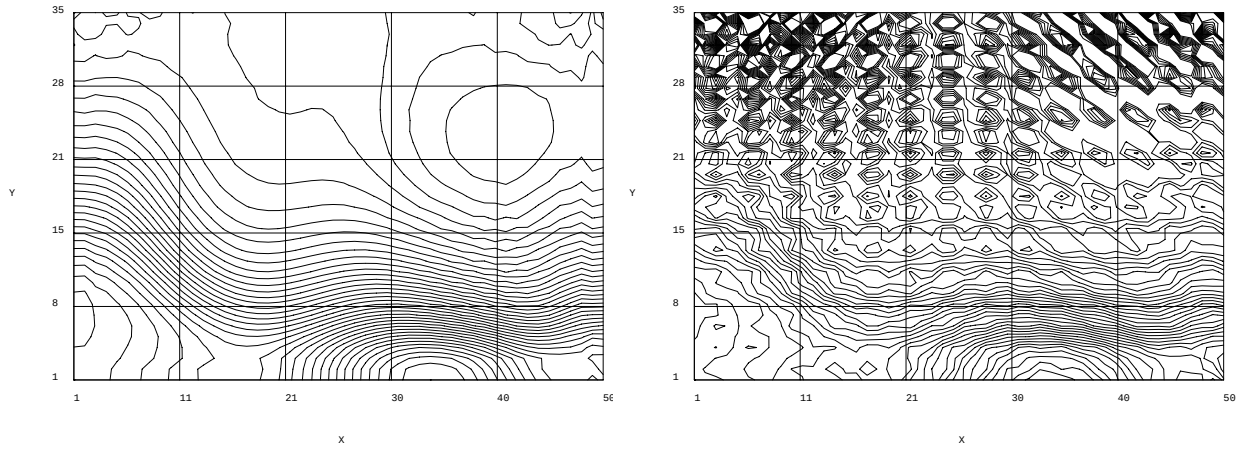

FIG. 2. *Cavity flow* $\mathrm{Re} = 500$ *pressure contours at* $z = 0.5$*: l) RLBE, r) LBGK*

high grid Reynolds number $\mathrm{Re}^* \equiv U/\nu = 40$, the pressure field still bears useful information, at least at some distance from the top corner singularities, as shown in figure 4. In contrast, the LBGK simulation at $\mathrm{Re} = 2000$ did not converge due to severe oscillations. With further increase of the Reynolds number to 4000 ($\nu = 0.00125$), the flow field becomes unsteady and complex three dimensional vortex shedding are observed. Detailed analysis of the flow will be published elsewhere.

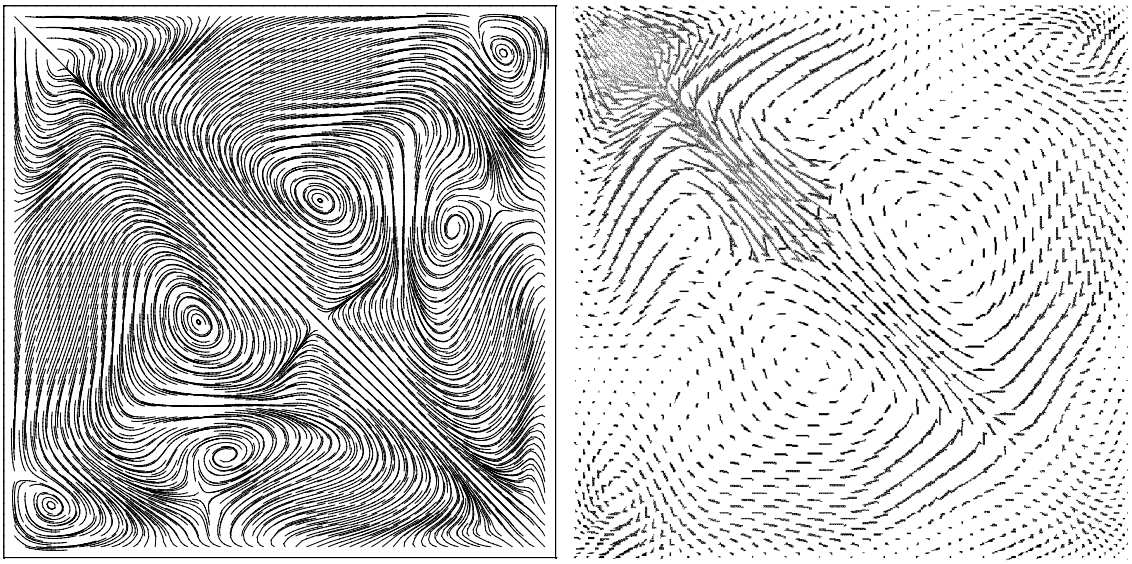

FIG. 3. *Cavity flow* $\mathrm{Re} = 2000$ *stream lines at* $y = 0.5$*: l) RLBE* 52^3 *uniform grids, r) FLUENT* 101^3 *non-uniform grids.*

In the simulations, suitable coding techniques should be applied to optimize the computational efficiency of the code. First and foremost, one should not use matrix calculations in the transformations between space $\mathbb{V}$ and space $\mathbb{M}$, instead, the transformations should be carried out explicitly using the formulae mapping $|f\rangle$ to $|m\rangle$ and *vice versa* (equations (2.2) and (2.4)). Secondly, the equilibria must be computed in moment space $\mathbb{M}$ and not in velocity space $\mathbb{V}$: this is the reason why we do not provide the equilibrium distribution functions $f_\alpha^{(\mathrm{eq})}$. Thirdly, all the common sub-expressions should be computed only once. This can be achieved either by explicitly computing these sub-expressions as separate variables or by carefully putting them between

parentheses and trusting modern compilers to do themselves the sub-expression reduction. Various compiler optimization options can easily accomplish this. Finally the use of $\rho_0 = 1$ instead of ρ avoids the need of a division in the calculations of the equilibria, and the use of $\delta\rho$ instead of ρ to increase numerical accuracy.

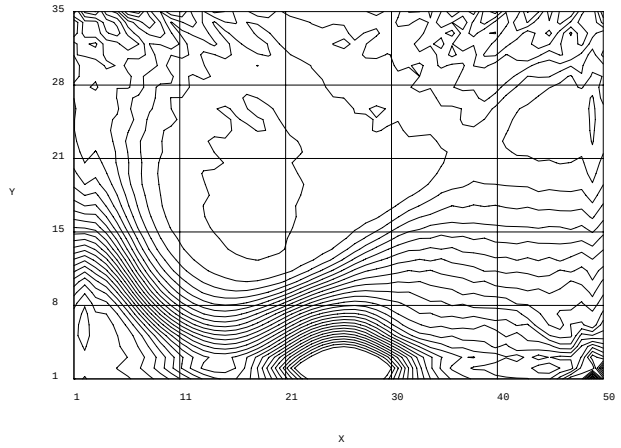

FIG. 4. *Cavity flow* $\mathrm{Re} = 2000$ *pressure contours at* $z = 0.5$, *RLBE* 52^3 *uniform grids*

By following these basic practices based on common sense, the number of operations required for the simulation of the multiple-relaxation-time D3Q15 model can be reduced to less than 120 additions/subtractions and 40 multiplications per time step on a grid point, as opposed to 80 additions/subtractions and 40 multiplications for the LBGK scheme with the same optimization effort. (The purpose of this counting is not to find the exact lower bounds, but only to have an estimate.) We would also like to stress that on modern computers the computational performance of lattice Boltzmann schemes is mostly limited by the available memory bandwidth and that rather soon the cost of local floating-point operations will be negligible. For instance, combining the collision and propagation steps into one loop would reduce about 1/3 of the time, because use of two loops doubles the memory access time. (However, this combination of loops is difficult to implement on vector machines.) With the optimization except the combination of collision and propagation together, the number of sites updated per second of the RLBE D3Q15 scheme for our test carried out on one node (8 processors) of a Hitachi SR-8000 parallel vector machine is about $1.76 \cdot 10^7$ as opposed to $2.06 \cdot 10^7$ for the LBGK D3Q15 scheme: the RLBE scheme is about 17% slower than the LBGK counterpart. The achieved FLOPS rate is 3.18 GFLOPS for the RLBE scheme versus 2.70 GFLOPS for the LBGK scheme. However it is important to note that, with the same computational effort and near the limit of numerical stability, the results obtained by using the RLBE scheme is much more accurate than the results obtained by using the LBGK scheme which are contaminated by numerical instability.

Free of the parity invariance, the D3Q19 RLBE model (see Appendix) further improves the stability. We have tested the D3Q19 RLBE model in the Povitsky cavity flow [28]. We used the 'link' bounce-back boundary conditions for the five walls and the correct boundary condition of equation (4.2) for the moving lid. With the same resolution of 51^3, the results obtained by using the D3Q19 RLBE model are much more accurate than that obtained by using the D3Q15 RLBE model with different boundary conditions. This confirms the previous observation that the D3Q19 LBGK model is more stable than the D3Q15 LBGK model [27]. A further comparative study of these two RLBE models is left for future work.

5. Conclusions. In this paper we provide a synopsis of the multiple-relaxation-time LBE in three dimensions and demonstrate its superior numerical stability and efficiency through the simulation of the

diagonally lid-driven cavity flow in three dimensions. The flow is geometrically simple, steady, and yet non-trivial. For this flow we estimate that the improvement in stability brought by the RLBE scheme yields an about four-fold gain in maximum Reynolds number when compared to the LBGK scheme. Of course, this improvement would be flow and boundary and initial condition dependent. Given that the computational effort required to solve time-dependent flows in three dimensions is basically proportional to Re^3, the stability improvement by using the RLBE scheme would reduce the computational effort by *at least* one order of magnitude while maintaining the accuracy of the simulations.

Acknowledgments. We are grateful to Dr. R. Rubinstein for his careful reading of the manuscript. MK acknowledges the technical support from the Leibniz-Rechenzentrum München. LSL is partially supported by the United States Air Force Office for Scientific Research under Grant No. F49620-01-1-0142 (technical monitor: Dr. J. Tishkoff).

Appendix A. Multiple-relaxation-time D3Q19 model.

The nineteen discrete velocities in D3Q19 models are:

$$\boldsymbol{e}_\alpha = \begin{cases} (0,\,0,\,0), & \alpha = 0, \\ (\pm 1,\,0,\,0),\ (0,\,\pm 1,\,0),\ (0,\,0,\,\pm 1), & \alpha = 1,\ 2,\ \ldots,\ 6, \\ (\pm 1,\,\pm 1,\,0),\ (\pm 1,\,0,\,\pm 1),\ (0,\,\pm 1,\,\pm 1), & \alpha = 7,\ 8,\ \ldots,\ 18, \end{cases} \tag{A.1}$$

and the components of the nineteen orthogonal basis vectors are given by

$$\left.\begin{aligned} |\phi_0\rangle_\alpha &= \|\boldsymbol{e}_\alpha\|^0 = 1, \\ |\phi_1\rangle_\alpha &= 19\|\boldsymbol{e}_\alpha\|^2 - 30, \\ |\phi_2\rangle_\alpha &= (21\|\boldsymbol{e}_\alpha\|^4 - 53\|\boldsymbol{e}_\alpha\|^2 + 24)/2, \end{aligned}\right\} \tag{A.2a}$$

$$\left.\begin{aligned} |\phi_3\rangle_\alpha &= e_{\alpha x}, \\ |\phi_5\rangle_\alpha &= e_{\alpha y}, \\ |\phi_7\rangle_\alpha &= e_{\alpha z}, \end{aligned}\right\} \tag{A.2b}$$

$$\left.\begin{aligned} |\phi_4\rangle_\alpha &= (5\|\boldsymbol{e}_\alpha\|^2 - 9)e_{\alpha x}, \\ |\phi_6\rangle_\alpha &= (5\|\boldsymbol{e}_\alpha\|^2 - 9)e_{\alpha y}, \\ |\phi_8\rangle_\alpha &= (5\|\boldsymbol{e}_\alpha\|^2 - 9)e_{\alpha z}, \end{aligned}\right\} \tag{A.2c}$$

$$\left.\begin{aligned} |\phi_9\rangle_\alpha &= 3e_{\alpha x}^2 - \|\boldsymbol{e}_\alpha\|^2, \\ |\phi_{11}\rangle_\alpha &= e_{\alpha y}^2 - e_{\alpha z}^2, \end{aligned}\right\} \tag{A.2d}$$

$$\left.\begin{aligned} |\phi_{13}\rangle_\alpha &= e_{\alpha x}e_{\alpha y}, \\ |\phi_{14}\rangle_\alpha &= e_{\alpha y}e_{\alpha z}, \\ |\phi_{15}\rangle_\alpha &= e_{\alpha x}e_{\alpha z}, \end{aligned}\right\} \tag{A.2e}$$

$$\left.\begin{aligned} |\phi_{10}\rangle_\alpha &= (3\|\boldsymbol{e}_\alpha\|^2 - 5)\,(3e_{\alpha x}^2 - \|\boldsymbol{e}_\alpha\|^2), \\ |\phi_{12}\rangle_\alpha &= (3\|\boldsymbol{e}_\alpha\|^2 - 5)\,(e_{\alpha y}^2 - e_{\alpha z}^2), \end{aligned}\right\} \tag{A.2f}$$

$$\left.\begin{aligned} |\phi_{16}\rangle_\alpha &= (e_{\alpha y}^2 - e_{\alpha z}^2)e_{\alpha x}, \\ |\phi_{17}\rangle_\alpha &= (e_{\alpha z}^2 - e_{\alpha x}^2)e_{\alpha y}, \\ |\phi_{18}\rangle_\alpha &= (e_{\alpha x}^2 - e_{\alpha y}^2)e_{\alpha z}, \end{aligned}\right\} \tag{A.2g}$$

where $\alpha \in \{0,\,1,\,\ldots,18\}$. The corresponding nineteen moments $\{m_\beta | \beta = 0,\ 1,\ \ldots,\ 18\}$ are arranged in the following order:

$$|m\rangle = (\rho, e, \epsilon, j_x, q_x, j_y, q_y, j_z, q_z, 3p_{xx}, 3\pi_{xx},\ p_{ww}, \pi_{ww}, p_{xy}, p_{yz}, p_{xz}, m_x, m_y, m_z)^{\mathsf{T}}.$$

There are fourteen vectors in the orthogonal basis set $\{|\phi_\beta\rangle\}$ with the same physical significance of the basis vectors in the D3Q15 model except for $|\phi_{14}\rangle$. These fourteen vectors correspond to the following moments: ρ, e, ϵ, $\boldsymbol{j}$, $\boldsymbol{q}$, and p_{ij}. In the D3Q19 basis set $\{|\phi_\beta\rangle\}$ there is no vector corresponding to the moment m_{xyz} of equation (3.2f). Instead, there are five vectors which are not in the D3Q15 basis set: three vectors of cubic order ($|\phi_{16}\rangle$, $|\phi_{17}\rangle$, and $|\phi_{18}\rangle$) and two of quartic order ($|\phi_{10}\rangle$ and $|\phi_{12}\rangle$). These five vectors are polynomials in $|\phi_3\rangle$, $|\phi_5\rangle$, and $|\phi_7\rangle$. The two vectors of quartic order, $|\phi_{10}\rangle$ and $\phi_{12}\rangle$, have the same symmetry as the diagonal part of the traceless tensor p_{ij}, while other three vectors of cubic order are parts of a third rank tensor, with the symmetry of $j_k p_{nm}$.

The diagonal collision matrix $\widehat{\mathsf{S}}$ is

$$\widehat{\mathsf{S}} \equiv \mathrm{diag}(0, s_1, s_2, 0, s_4, 0, s_4, 0, s_4, s_9, s_{10}, s_9, s_{10}, s_{13}, s_{13}, s_{13}, s_{16}, s_{16}, s_{16}),$$

and the transformation matrix M is given at the end of this appendix. Again, the 4th, 6th, and 8th row vectors of M (corresponding to j_x, j_y, and j_z, respectively) uniquely define the ordering (or labelling) of the velocity set $\{\boldsymbol{e}_\alpha\}$ with respect to subscript α.

With $c_s^2 = 1/3$ and $s_9 = s_{13}$, the equilibria of the non-conserved moments are given as functions up to second-order in ρ and $\boldsymbol{j}$ as follows:

$$e^{(\mathrm{eq})} = -11\rho + \frac{19}{\rho_0}\boldsymbol{j}\cdot\boldsymbol{j} = -11\rho + \frac{19}{\rho_0}(j_x^2 + j_y^2 + j_z^2), \tag{A.3a}$$

$$\epsilon^{(\mathrm{eq})} = w_\epsilon\,\rho + \frac{w_{\epsilon j}}{\rho_0}\,\boldsymbol{j}\cdot\boldsymbol{j}, \tag{A.3b}$$

$$q_x^{(\mathrm{eq})} = -\frac{2}{3}j_x, \qquad q_y^{(\mathrm{eq})} = -\frac{2}{3}j_y, \qquad q_z^{(\mathrm{eq})} = -\frac{2}{3}j_z, \tag{A.3c}$$

$$p_{xx}^{(\mathrm{eq})} = \frac{1}{3\rho_0}\left[2j_x^2 - (j_y^2 + j_z^2)\right], \qquad p_{ww}^{(\mathrm{eq})} = \frac{1}{\rho_0}\left[j_y^2 - j_z^2\right], \tag{A.3d}$$

$$p_{xy}^{(\mathrm{eq})} = \frac{1}{\rho_0}j_x j_y, \qquad p_{yz}^{(\mathrm{eq})} = \frac{1}{\rho_0}j_y j_z, \qquad p_{xz}^{(\mathrm{eq})} = \frac{1}{\rho_0}j_x j_z, \tag{A.3e}$$

$$\pi_{xx}^{(\mathrm{eq})} = w_{xx}p_{xx}^{(\mathrm{eq})}, \qquad \pi_{ww}^{(\mathrm{eq})} = w_{xx}p_{ww}^{(\mathrm{eq})}, \tag{A.3f}$$

$$m_x^{(\mathrm{eq})} = m_y^{(\mathrm{eq})} = m_z^{(\mathrm{eq})} = 0, \tag{A.3g}$$

where w_ϵ and $w_{\epsilon j}$ are again free parameters and w_{xx} is an additional free parameter in the D3Q19 model.

The bulk viscosity ζ of the D3Q19 model is equal to that of the D3Q15 model given in equation (3.6b) and its kinematic viscosity ν is

$$\nu = \frac{1}{3}\left(\frac{1}{s_9} - \frac{1}{2}\right) = \frac{1}{3}\left(\frac{1}{s_{13}} - \frac{1}{2}\right). \tag{A.4}$$

To recover the corresponding LBGK model, one must set $w_\epsilon = 3$, $w_{\epsilon j} = -11/2$, and $w_{xx} = -1/2$. However, to attain an optimized stability of the model, we obtained the following parameter values through linear analysis (Lallemand & Luo 2000): $w_\epsilon = 0$, $w_{\epsilon j} = -475/63$, $w_{xx} = 0$, $s_1 = 1.19$, $s_2 = s_{10} = 1.4$, $s_4 = 1.2$, and $s_{16} = 1.98$. With the above parameter values, we can use a maximum speed of 0.19 (Mach number M ≈ 0.33) and a viscosity $\nu > 2.54\cdot 10^{-3}$ in simulations. The linear analysis to obtain these 'optimal' parameter values is a local analysis of a system with a uniform velocity of wave-vector $\boldsymbol{k}$. The local analysis does not consider boundary conditions and therefore the system may be less stable in actual simulations.

The transformation matrix M is given by

$$\mathsf{M} = \begin{vmatrix}
1 & 1 & 1 & 1 & 1 & 1 & 1 & 1 & 1 & 1 & 1 & 1 & 1 & 1 & 1 & 1 & 1 & 1 & 1 \\
-30 & -11 & -11 & -11 & -11 & -11 & -11 & 8 & 8 & 8 & 8 & 8 & 8 & 8 & 8 & 8 & 8 & 8 & 8 \\
12 & -4 & -4 & -4 & -4 & -4 & -4 & 1 & 1 & 1 & 1 & 1 & 1 & 1 & 1 & 1 & 1 & 1 & 1 \\
0 & 1 & -1 & 0 & 0 & 0 & 0 & 1 & -1 & 1 & -1 & 1 & -1 & 1 & -1 & 0 & 0 & 0 & 0 \\
0 & -4 & 4 & 0 & 0 & 0 & 0 & 1 & -1 & 1 & -1 & 1 & -1 & 1 & -1 & 0 & 0 & 0 & 0 \\
0 & 0 & 0 & 1 & -1 & 0 & 0 & 1 & 1 & -1 & -1 & 0 & 0 & 0 & 0 & 1 & -1 & 1 & -1 \\
0 & 0 & 0 & -4 & 4 & 0 & 0 & 1 & 1 & -1 & -1 & 0 & 0 & 0 & 0 & 1 & -1 & 1 & -1 \\
0 & 0 & 0 & 0 & 0 & 1 & -1 & 0 & 0 & 0 & 0 & 1 & 1 & -1 & -1 & 1 & 1 & -1 & -1 \\
0 & 0 & 0 & 0 & 0 & -4 & 4 & 0 & 0 & 0 & 0 & 1 & 1 & -1 & -1 & 1 & 1 & -1 & -1 \\
0 & 2 & 2 & -1 & -1 & -1 & -1 & 1 & 1 & 1 & 1 & 1 & 1 & 1 & 1 & -2 & -2 & -2 & -2 \\
0 & -4 & -4 & 2 & 2 & 2 & 2 & 1 & 1 & 1 & 1 & 1 & 1 & 1 & 1 & -2 & -2 & -2 & -2 \\
0 & 0 & 0 & 1 & 1 & -1 & -1 & 1 & 1 & 1 & 1 & -1 & -1 & -1 & -1 & 0 & 0 & 0 & 0 \\
0 & 0 & 0 & -2 & -2 & 2 & 2 & 1 & 1 & 1 & 1 & -1 & -1 & -1 & -1 & 0 & 0 & 0 & 0 \\
0 & 0 & 0 & 0 & 0 & 0 & 0 & 1 & -1 & -1 & 1 & 0 & 0 & 0 & 0 & 0 & 0 & 0 & 0 \\
0 & 0 & 0 & 0 & 0 & 0 & 0 & 0 & 0 & 0 & 0 & 0 & 0 & 0 & 0 & 1 & -1 & -1 & 1 \\
0 & 0 & 0 & 0 & 0 & 0 & 0 & 0 & 0 & 0 & 0 & 1 & -1 & -1 & 1 & 0 & 0 & 0 & 0 \\
0 & 0 & 0 & 0 & 0 & 0 & 0 & 1 & -1 & 1 & -1 & -1 & 1 & -1 & 1 & 0 & 0 & 0 & 0 \\
0 & 0 & 0 & 0 & 0 & 0 & 0 & -1 & -1 & 1 & 1 & 0 & 0 & 0 & 0 & 1 & -1 & 1 & -1 \\
0 & 0 & 0 & 0 & 0 & 0 & 0 & 0 & 0 & 0 & 0 & 1 & 1 & -1 & -1 & -1 & -1 & 1 & 1
\end{vmatrix}. \tag{A.5}$$

REFERENCES

[1] P.L. Bhatnagar, E.P. Gross, and M. Krook, *A model for collision processes in gases. I. Small amplitude processes in charged and neutral one-component system*, Phys. Rev., 94 (1954), pp. 511–525.

[2] M. Bouzidi, D. d'Humières, P. Lallemand, and L.-S. Luo, *Lattice Boltzmann equation on a two-dimensional rectangular grid*, J. Computat. Phys., 172 (2001), pp. 704–717.

[3] M. Bouzidi, M. Firdaouss, and P. Lallemand, *Momentum transfer of a Boltzmann-lattice fluid with boundaries*, Phys. Fluids, 13 (2001), pp. 452–459.

[4] H. Chen, S. Chen, and W.H. Matthaeus, *Recovery of the Navier-Stokes equations using a lattice-gas Boltzmann method*, Phys. Rev. A, 45 (1992), pp. R5339–R5342.

[5] R. Cornubert, *Conditions aux limites des modèles cinétiques discrets: Couche de Knudsen et obstacles*, Ph.D. thesis, Université Pierre et Marie Curie, Paris, 1991.

[6] R. Cornubert, D. d'Humières, and D. Levermore, *A Knudsen layer theory for lattice gases*, Physica D, 47 (1991), pp. 241–259.

[7] D. d'Humières, *Generalized lattice-Boltzmann equation*, in *Rarefied Gas Dynamics: Theory and Simulations*, *Progress in Astronautics and Aeronautics* Vol. 159, edited by B. D. Shizgal and D. P. Weaver AIAA, Washington, DC, 1992, pp. 450–458.

[8] D. d'Humières, M. Bouzidi, and P. Lallemand, *Thirteen-velocity three-dimensional lattice Boltzmann model*, Phys. Rev. E, 63 (2001), pp. 066702-1–7.

[9] I. Ginzburg, *Introduction of upwind and free boundary into lattice Boltzmann method*, in *Discrete Modelling and Discrete Algorithms in Continuum Mechanics*, edited by Th. Sonar and I. Thomas

Logos-Verlag, Berlin, 2001, pp. 97–110.

[10] I. Ginzbourg and P.M. Alder, *Boundary flow condition analysis for the three-dimensional lattice Boltzmann model*, J. Phys. II, 4 (1994), pp. 191–214.

[11] I. Ginzbourg and P.M. Alder, *Surface tension models with different viscosities*, Transport in Porous Media, 20 (1995), pp. 37–76.

[12] I. Ginzbourg and K. Steiner, *Free surface lattice-Boltzmann method to model the filling of expanding cavities by Bingham fluids*, Phil. Trans. R. Soc. Lond. A, 360 (2002), pp. 453–466.

[13] L. Giraud, D. d'Humières, and P. Lallemand, *A lattice Boltzmann model for viscoelasticity*, Int. J. Mod. Phys. C, 8 (1997), pp. 805–815.

[14] ——, *A lattice Boltzmann model for Jeffreys viscoelastic fluid*, Europhys. Lett., 42 (1998), pp. 625–630.

[15] H. Grad, *Principles of the kinetic theory of gases*, in *Encyclopedia of Physics*, edited by S. Flügge, Vol. XII, *Thermodynamics of Gases*, Springer-Verlag, Berlin, 1958, pp. 205–294.

[16] S. Harris, *An Introduction to the Theory of the Boltzmann Equation*, Holt, Rinehart & Winston, New York, 1971.

[17] X. He and L.-S. Luo, *A priori derivation of the lattice Boltzmann equation*, Phys. Rev. E, 55 (1997), pp. R6333–R6336.

[18] ——, *Theory of the lattice Boltzmann method: From the Boltzmann equation to the lattice Boltzmann equation*, Phys. Rev. E, 56 (1997), pp. 6811–6817.

[19] ——, *Lattice Boltzmann model for the incompressible Navier-Stokes equation*, J. Stat. Phys., 88, (1997), pp. 927–944.

[20] F.J. Higuera and J. Jeménez, *Boltzmann approach to lattice gas simulations*, Europhys. Lett., 9 (1989), pp. 663–668.

[21] F.J. Higuera, S. Succi, and R. Benzi, *Lattice Gas-Dynamics with Enhanced Collisions*, Europhys. Lett., 9 (1989), pp. 345–349.

[22] A.J.C. Ladd, *Numerical simulations of particulate suspensions via a discretized Boltzmann equation. Part 1. Theoretical foundation*, J. Fluid Mech., 271 (1994), pp. 285–309

[23] P. Lallemand and L.-S. Luo, *Theory of the lattice Boltzmann method: Dispersion, dissipation, isotropy, Galilean invariance, and stability*, Phys. Rev. E, 61 (2000), pp. 6546–6562.

[24] L.-S. Luo, *Unified Theory of the lattice Boltzmann models for nonideal gases*, Phys. Rev. Lett., 81 (1998), pp. 1618–1621.

[25] L.-S. Luo, *Theory of the lattice Boltzmann method: Lattice Boltzmann models for nonideal gases*, Phys. Rev. E, 62 (2000), pp. 4982–4996.

[26] G.R. McNamara, A.L. Garcia, and B.J. Alder, *Stabilization of thermal lattice Boltzmann models*, J. Stat. Phys., 81 (1995), pp. 395–408.

[27] R. Mei, W. Shyy, D. Yu, and L.-S. Luo, *Lattice Boltzmann method for 3-d flows with curved boundary*, J. Comput. Phys., 161 (2000), pp. 680–699.

[28] A. Povitsky, *High-incidence 3-D lid-driven cavity flow*, American Institute of Aeronautics and Astronautics, AIAA Paper 01-2847 (2001), pp. 1–7.

[29] Y.H. Qian, D. d'Humires, and P. Lallemand, *Lattice BGK models for Navier-Stokes equation*, Europhys. Lett., 17 (1992), pp. 479–484.

[30] G. Zanetti, *The hydrodynamics of lattice gas automata*, Phys. Rev. A, 40 (1989), pp. 1539–1548.

REPORT DOCUMENTATION PAGE

Form Approved
OMB No. 0704-0188

1. AGENCY USE ONLY *(Leave blank)*	2. REPORT DATE	3. REPORT TYPE AND DATES COVERED
	July 2002	Contractor Report

4. TITLE AND SUBTITLE
MULTIPLE-RELAXATION-TIME LATTICE BOLTZMANN MODELS IN 3D

5. FUNDING NUMBERS
C NAS1-97046
WU 505-90-52-01

6. AUTHOR(S)
Dominique d'Humieres, Irina Ginzburg, Manfred Krafczyk, Pierre Lallemand, and Li-Shi Luo

7. PERFORMING ORGANIZATION NAME(S) AND ADDRESS(ES)
ICASE
Mail Stop 132C
NASA Langley Research Center
Hampton, VA 23681-2199

8. PERFORMING ORGANIZATION REPORT NUMBER
ICASE Report No. 2002-20

9. SPONSORING/MONITORING AGENCY NAME(S) AND ADDRESS(ES)
National Aeronautics and Space Administration
Langley Research Center
Hampton, VA 23681-2199

10. SPONSORING/MONITORING AGENCY REPORT NUMBER
NASA/CR-2002-211660
ICASE Report No. 2002-20

11. SUPPLEMENTARY NOTES
Langley Technical Monitor: Dennis M. Bushnell
Final Report
To appear in the Proceedings of the Royal Society London A.

12a. DISTRIBUTION/AVAILABILITY STATEMENT
Unclassified–Unlimited
Subject Category 34
Distribution: Nonstandard
Availability: NASA-CASI (301) 621-0390

12b. DISTRIBUTION CODE

13. ABSTRACT *(Maximum 200 words)*
This article provides a concise exposition of the multiple-relaxation-time lattice Boltzmann equation, with examples of fifteen-velocity and nineteen-velocity models in three dimensions. Simulation of a diagonally lid-driven cavity flow in three dimensions at Re=500 and 2000 is performed. The results clearly demonstrate the superior numerical stability of the multiple-relaxation-time lattice Boltzmann equation over the popular lattice Bhatnagar-Gross-Krook equation.

14. SUBJECT TERMS
multiple-relaxation-time LBE in 3D, D3Q15 and D3Q19 models, 3D diagonal lid driven cavity flow

15. NUMBER OF PAGES
18

16. PRICE CODE
A03

17. SECURITY CLASSIFICATION OF REPORT	18. SECURITY CLASSIFICATION OF THIS PAGE	19. SECURITY CLASSIFICATION OF ABSTRACT	20. LIMITATION OF ABSTRACT
Unclassified	Unclassified		